Investigation of Ring-heterogeneous Geometry Approximation for Efficient and Practical SFR Analysis

April 2024

Changing the World's Energy Future

Namjae Choi, Stefano Terlizzi, Yaqi Wang, Hansol Park, Chang-ho Lee, Javier Ortensi

Idaho National Laboratory

Investigation of Ring-heterogeneous Geometry Approximation for Efficient and Practical SFR Analysis

Namjae Choi, Stefano Terlizzi, Yaqi Wang, Hansol Park, Chang-ho Lee, Javier Ortensi

April 2024

Idaho National Laboratory
Idaho Falls, Idaho 83415

http://www.inl.gov

Investigation of Ring-heterogeneous Geometry Approximation
for Efficient and Practical SFR Analysis

Namjae Choi[1], Stefano Terlizzi[1], Yaqi Wang[1], Hansol Park[2], Changho Lee[2], Javier Ortensi[1]*

[1]Idaho National Laboratory, 1955 N. Fremont Ave., Idaho Falls, ID 83415
[2]Argonne National Laboratory, 9700 S. Cass Ave., Lemont, IL 60439

ABSTRACT

A novel geometry approximation scheme named ring-heterogeneous approximation for intermediate resolution multiphysics analysis of SFRs is presented. This approach particularly targets neutronics coupled with thermo-mechanics feedback, which dominate the passive safety of SFR designs. The ring-heterogeneous approximation casts an array of pins into volume-preserving bands of materials that constitute the pins. It allows to efficiently simulate SFRs with an unstructured mesh and also to explicitly consider the deformation of each material by retaining their heterogeneity. Verification results with single assembly and core problems of the ABTR benchmark demonstrated that the ring-heterogeneous approximation is a reasonable approximation for SFRs. For a 2D full core problem, the ring-heterogeneous approximation significantly reduced the number of elements by at least a factor of 70 from a fully-heterogeneous mesh while almost exactly preserving the reference fully-heterogeneous solutions with the RMS error of only 0.02% in the ring-wise fission reaction rate.

Keywords: SFR, ABTR, MOOSE, Griffin, Ring-heterogeneous

1.   INTRODUCTION

The past few years have seen a resurgence of global interest in advanced reactors including sodium-cooled fast reactors (SFR), amid a flood of plans by governments and private companies to develop and deploy advanced reactors including TerraPower's Natrium™ reactor [1]. Consequently, the necessity and demand for modeling and simulation tools for advanced reactors are higher than ever.

Idaho National Laboratory (INL) is working closely with the U.S. Nuclear Regulatory Commission (NRC) to support the deployment of advanced reactors by developing modeling and simulation tools for advanced reactors under the support of the Nuclear Energy Advanced Modeling and Simulation (NEAMS) program of the U.S. Department of Energy (DOE). Among the NEAMS tools, Griffin [2] is the neutronics analysis code targeted for the analysis of advanced reactors, and it is built upon the MOOSE (Multiphysics Object-Oriented Simulation Environment) framework [3]. Multiphysics analyses of various advanced reactors are currently being performed using Griffin coupled with other MOOSE-based multiphysics codes [4, 5, 6], and the neutronics/thermal-hydraulics/thermo-mechanics coupled multiphysics analysis of SFRs is one of the important activities.

This paper introduces the ring-heterogeneous geometry approximation scheme being employed in Griffin for efficient and practical SFR multiphysics analysis and presents its verification. The ring-heterogeneous

---

* Corresponding author: Javier.Ortensi@inl.gov

approximation was designed to significantly reduce the number of elements in the mesh compared to the fully-heterogeneous mesh, while retaining the heterogeneity between each material such as fuel, cladding, sodium, duct, etc. It allows an explicit deformation of each material, which can capture the most important thermo-mechanical feedback mechanisms in SFRs related to volume expansion. In the following section, the ring-heterogeneous approximation will be introduced schematically with rationales, and in Section 3, its verification will be presented for single assembly and full core problems with fully-heterogeneous and Monte Carlo solutions as the references. Lastly, conclusions will be drawn at the end.

2.   RING-HETEROGENEOUS GEOMETRY APPROXIMATION

The necessity of an efficient yet accurate geometry approximation scheme stems from the fact that Griffin is a finite element code employing a general unstructured mesh. Unstructured meshes have strengths in that they provide flexibility in modeling irregular and complicated geometries frequently observed in research or advanced reactors, thus enabling straightforward coupling with multiphysics codes and direct geometry deformation simulations. However, they reveal issues in modeling large power reactors such as LWRs or SFRs. They contain tens of thousands of compactly loaded cylindrical fuel pins, and proper modeling of those geometries requires an extremely refined mesh. As the result, the number of elements can easily reach tens or hundreds of millions, which becomes computationally prohibitive. Many neutron transport codes implement tailored geometry modules targeting the regular lattice structure of those reactors and employ the method of characteristics (MOC) to perform pin-resolved whole-core transport calculations efficiently. However, tailored geometry treatments have limitations in simulating geometry deformations which is the most important feedback mechanism in SFRs, and MOC typically relies on approximations such as 2D/1D or 2D/3D methods to perform 3D calculations.

Hence, to retain the advantages of the unstructured mesh, which are the flexibility in geometry deformation and the ability to perform full 3D transport calculations using finite element methods while being able to simulate SFRs efficiently, the ring-heterogeneous geometry approximation was devised. Considering that each material must be able to be deformed explicitly to properly capture the thermo-mechanical feedback effects, the ring-heterogeneous approximation retains the heterogeneity between materials while reducing the number of elements significantly. In this aspect, the ring-heterogeneous approximation compares with the duct-heterogeneous approximation [7] where all the materials in an assembly are homogenized except the duct region. The duct-heterogeneous approximation can still explicitly model the radial displacement of assemblies by support plate deformation by retaining the heterogeneities in the duct region, but it has limitations in simulating the axial deformation of materials such as fuel or control rod drivelines separately, and it must resort to the functionalization of cross sections with respect to the axial deformation. The ring-heterogeneous approximation aims to eliminate such limitation.

Figure 2-1 schematically illustrates two ways of the ring-heterogeneous approximation investigated in this work: the exact ring-heterogeneous approximation and the simplified ring-heterogeneous approximation. The idea of ring-heterogeneous approximation is to cast an array of pin cells into the "bands" of materials constituting the pin cells (e.g., fuel, cladding, and coolant) while preserving their volumes. In a hexagonal geometry, the pin cells along each hexagon will be smeared into bands that resemble rings, after which the approximation scheme was named. The exact ring-heterogeneous approximation preserves the "topology" of the materials. In the figure, for instance, the topology that fuel is centered and surrounded by cladding and coolant is conserved. On the other hand, the simple ring-heterogeneous approximation makes a more aggressive approximation to minimize the number of elements: it only considers the number of materials and creates one band per material without considering their arrangement.

From now on, the exact ring-heterogeneous approximation will be simply called as the ring-heterogeneous approximation. Table I shows and compares the fully-heterogeneous (FH), ring-heterogeneous (RH), and simple ring-heterogeneous (SRH) meshes of a 2D single fuel assembly of the Advanced Burner Test Reactor

(ABTR) benchmark [8]. It can be seen that RH can significantly reduce the number of elements from FH by a factor of 40. SRH further reduces the number of elements from RH to two-thirds, but it makes the fuel bands more centered than the actual assembly configuration, and one side of a fuel band comes into contact with coolant directly while the other side sees a thicker cladding. This will alter the neutronic characteristics of the problem to some extent, whose impact will be investigated in this paper.
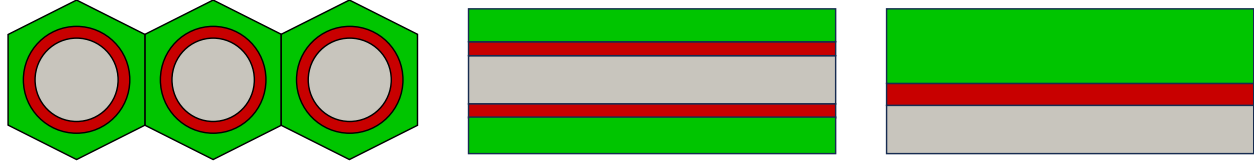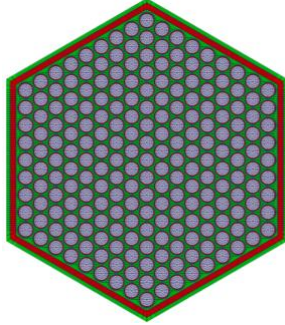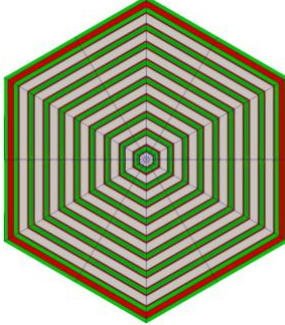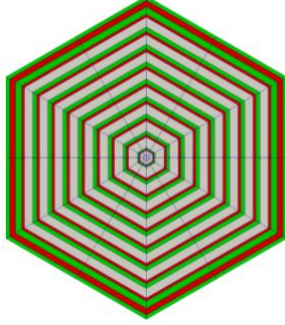

Figure 2-1. Schematic diagram of exact ring-heterogeneous (middle) and simple ring-heterogeneous (right) approximations of a fully-heterogeneous (left) geometry.

Table I. Comparison of FH, RH, and SRH meshes of a 2D ABTR fuel assembly.

Mesh	FH	RH	SRH
Geometry			
# Elements	22,056	546	354

3.   VERIFICATION RESULTS

This section presents the verification results of the ring-heterogeneous approximation schemes for the single assembly and full core problems of the ABTR benchmark. The cross sections were generated using MC^2-3 [9] in 9 groups (ANL9 group structure) at 855.65K, and this temperature is applied uniformly. For each case, fission and absorption reaction rates are compared as well as eigenvalues. Here, absorption excludes fission; namely, it is the sum of all reactions that do not produce neutrons. The reaction rate distributions are normalized to their volume average, and their errors are given as absolute differences in percent. All the Griffin calculations employed the first-order discontinuous finite element S_N (DFEM-S_N) method with 2 polar angles and 6 azimuthal angles per octant (Gauss-Chebyshev quadrature) and P_3 scattering.

3.1.   Single Assembly Verification

3.1.1.   2D single assembly

For 2D single assembly problems, the eigenvalues and ring-wise fission and absorption reaction rates of RH and SRH are compared with the FH results which are the reference. Table II reports the eigenvalues of

three types of fuel assemblies in ABTR, which differ in burnup and the plutonium enrichment, with three types of meshes, and Figure 3-1 and Figure 3-2 present the ring-wise fission and absorption reaction rate errors of RH and SRH. Here, each ring includes surrounding cladding and sodium as well as fuel.

RH yields almost exact eigenvalues with FH with less than 5 pcm errors, while SRH presents errors of 40 ~ 60 pcm. For the fission reaction rate, both RH and SRH show negligible errors of less than 0.12%. For the absorption reaction rate, however, SRH presents the maximum error of over 0.6% while that of RH is below 0.1%, which is considered to be the cause of the larger eigenvalue errors of SRH. The difference in the error behavior between fission and absorption reaction rates is due to the role of U-238 whose number density still accounts for more than 60% of the fuel. The fission reaction rate presents a very flat distribution as it is dominated by fast fission, while in the absorption reaction rate, the resonance absorption and self-shielding of U-238 becomes non-negligible. Self-shielding is strongly affected by the geometry, and thus SRH that does not preserve the topology of the original geometry incurs larger errors than RH specifically in the absorption reaction rates. Still, whether the degree of eigenvalue and absorption reaction rate errors of SRH is significant is questionable.

Table II. Comparison of eigenvalues between FH, RH, and SRH for the 2D single assemblies. The values in the parentheses are the errors against FH in pcm.

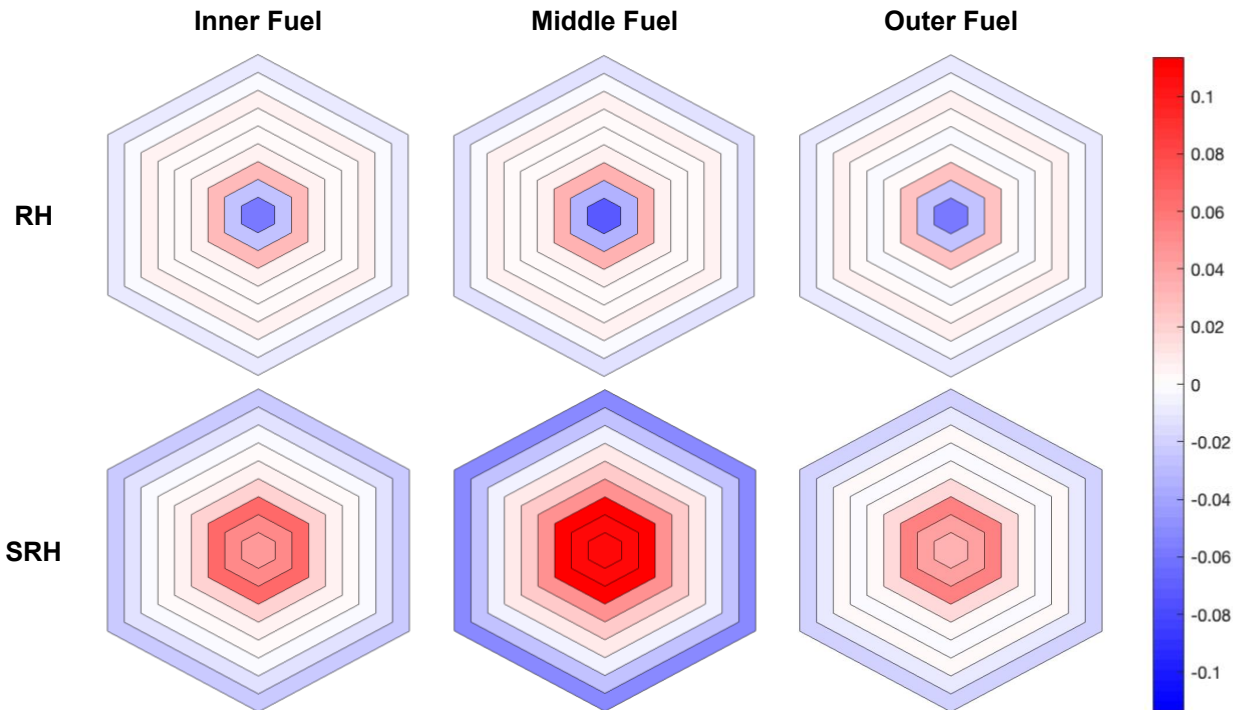| Case	FH	RH	SRH
Inner Fuel	1.55326	1.55331 (5)	1.55374 (48)
Middle Fuel	1.39217	1.39222 (5)	1.39275 (58)
Outer Fuel	1.71978	1.71982 (4)	1.72021 (43)

Figure 3-1. Ring-wise fission reaction rate errors (%) of RH and SRH against FH for the 2D single assemblies.
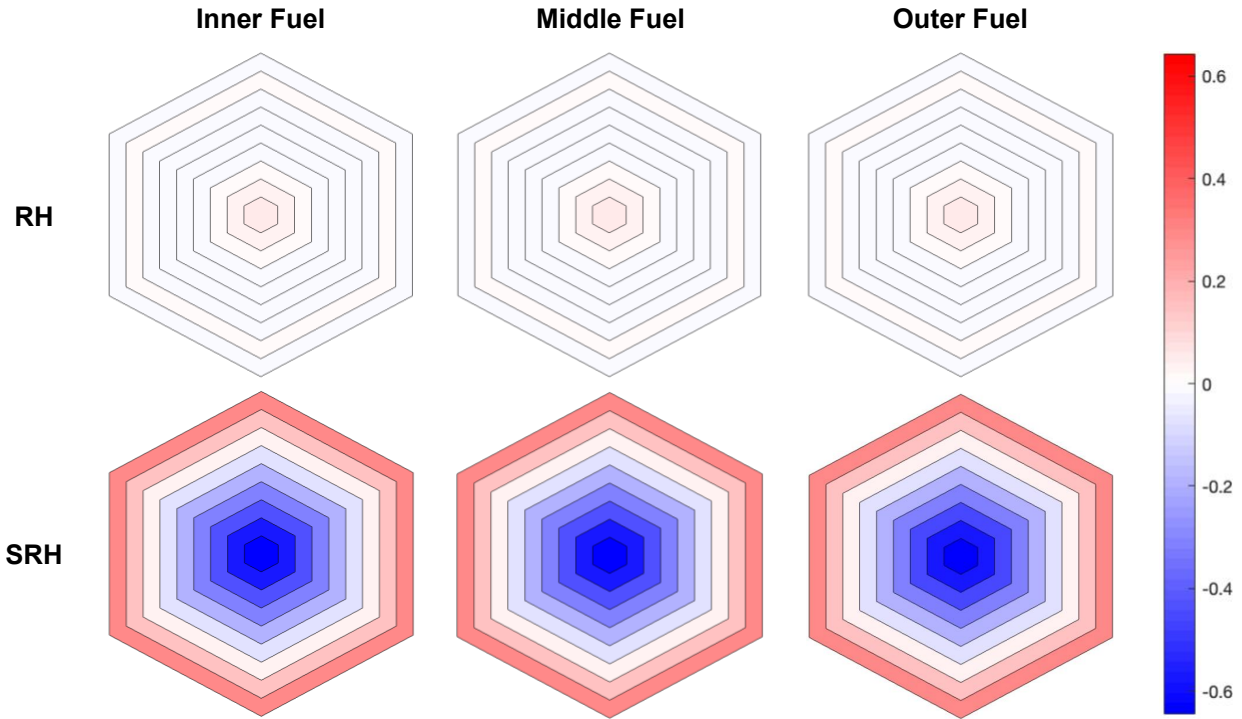
Figure 3-2. Ring-wise absorption reaction rate errors (%) of RH and SRH against FH for the 2D single assemblies.

3.1.2. 3D single assembly

For 3D single assembly problems, the eigenvalues and radially-integrated plane-wise fission and absorption reaction rates in the active core region are compared with the FH results. The axially-integrated ring-wise reaction rates present a very similar behavior with the 2D single assembly cases, so they are not repeated here. Table III reports the eigenvalues of the three types of fuel assemblies and meshes, and Figure 3-3 presents the plane-wise fission and absorption reaction rate errors of RH and SRH along with the reference reaction rates of FH.

The eigenvalues exhibit a very similar trend with the 2D single assembly cases: RH yields almost the same eigenvalues with FH while SRH shows tens of pcm errors. The cause of larger errors in SRH is also identical with the 2D single assembly cases. In terms of plane-wise reaction rates, although SRH tends to show larger errors, their magnitude is negligible. Thus, it is considered that both RH and SRH do not have a meaningful impact in the axial reaction rate distributions and that both approaches yield accurate solutions.

Table III. Comparison of eigenvalues between FH, RH, and SRH for the 3D single assemblies. The values in the parentheses are the errors against FH in pcm.

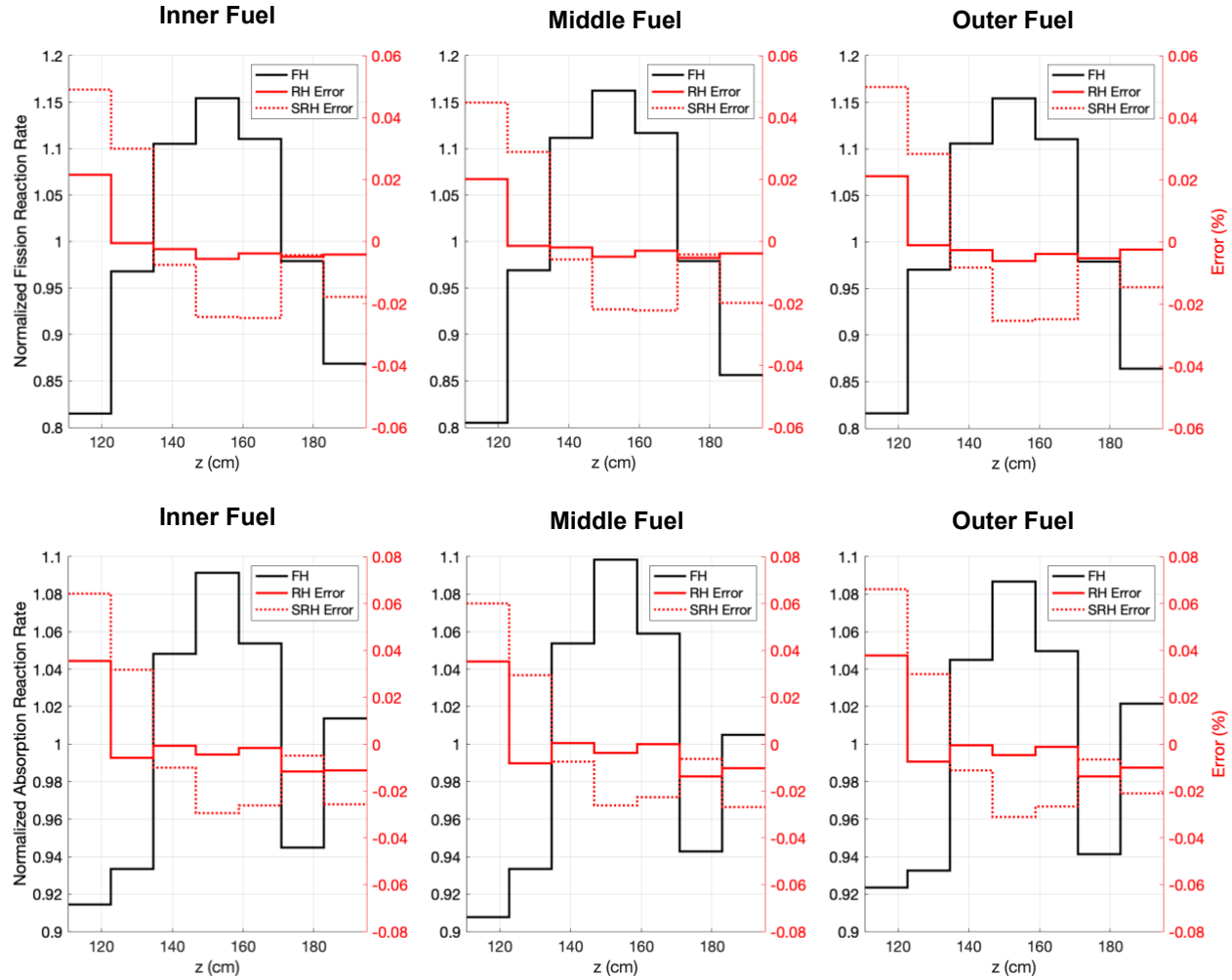| Case	FH	RH	SRH
Inner Fuel	1.34932	1.34935 (3)	1.34973 (41)
Middle Fuel	1.21408	1.21414 (6)	1.21464 (56)
Outer Fuel	1.50269	1.50272 (3)	1.50305 (36)

Figure 3-3. Radially-integrated plane-wise fission (top) and absorption (bottom) reaction rates of FH and errors (%) of RH and SRH against FH for the 3D single assemblies.

3.2. Full Core Verification

3.2.1. 2D full core

For the unrodded 2D full core problem, the eigenvalues and ring-wise fission and absorption reaction rates in the fuel assemblies are compared with the FH results. The FH mesh has 4,291,772 elements, while the RH and SRH meshes only have 61,444 and 47,872 elements, respectively. Table IV presents the eigenvalues of FH, RH, and SRH calculations, and Figure 3-4 shows the ring-wise fission and absorption reaction rate errors of RH and SRH against FH.

RH showcases almost exact agreement with FH in all the observed quantities. The eigenvalue error is only -19 pcm, and the degree of errors in the reaction rates remains at a comparable level with the single assembly problems: the maximum fission and absorption reaction rate errors are 0.10% and 0.08%, respectively, and the corresponding root mean square (RMS) errors are 0.02% and 0.01%, respectively, which are completely negligible. On the other hand, SRH exhibits larger errors overall. The eigenvalue error goes over 100 pcm, and the absorption reaction rate error is close to 1% in the maximum where the RMS error is 0.30%. The fission reaction rate error is smaller due to the nature of fast fission that it is not affected by self-shielding

much, whose maximum and RMS values are 0.34% and 0.16%, respectively. However, a global in-out tilt is observed in the error distribution, which indicates that SRH is affected by the global leakage in contrast to RH. In fact, while the errors seem large in a relative sense against RH, their magnitude itself is in a level which is generally considered insignificant. Still, this baseline error can be amplified in more challenging conditions such as rodded, transient, or multiphysics conditions, so more thorough investigations will be required for SRH to be utilized in such "irregular" conditions.

Table IV. Comparison of eigenvalues between FH, RH, and SRH for the 2D full core. The values in the parentheses are the errors against FH in pcm.

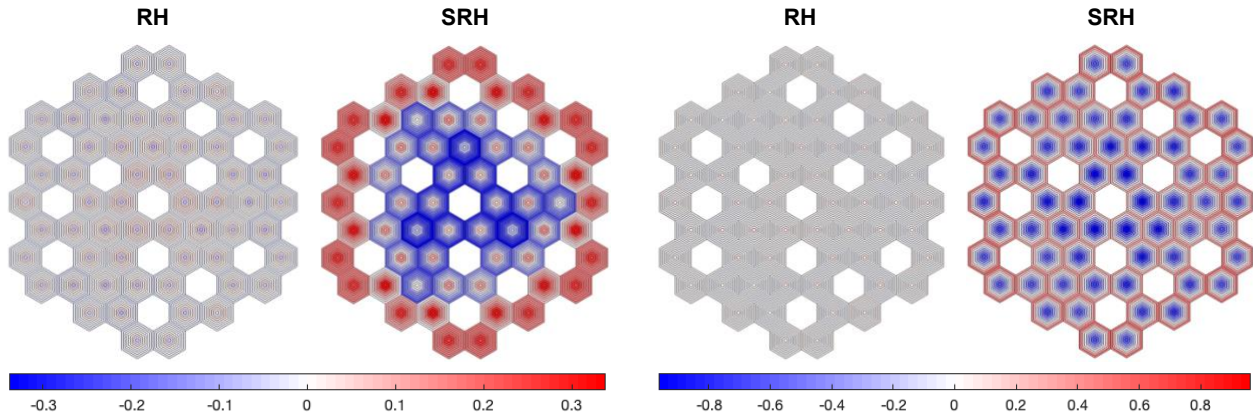| Case	FH	RH	SRH
Eigenvalue	1.23788	1.23769 (-19)	1.23905 (117)

Figure 3-4. Ring-wise fission (left) and absorption (right) reaction rate errors (%) of RH and SRH against FH for the 2D full core.

3.2.2. 3D full core

For the 3D full core problem, FH calculation requires a prohibitive amount of computational costs, so the RH and SRH solutions are compared with the Serpent [10] Monte Carlo (MC) solutions. Serpent employed 100 inactive cycles and 1,000 active cycles with 10 million particles per cycle, resulting in 10 billion active histories. Griffin was parallelized with 200 cores of Intel Xeon Gold 6148 CPUs. The RH and SRH meshes have 1,467,456 and 1,148,928 elements, respectively, and at these conditions, their runtimes were 28.8 and 24.3 minutes, respectively. While MOOSE is highly parallelizable and can leverage more CPU cores which might allow less geometry approximation, it is desired to limit the number of CPU cores for practicality as such massively parallel computing environments are not easily available to general users.

Table V reports the eigenvalues of MC, RH, and SRH calculations, and Figure 3-5 illustrates the axially-integrated ring-wise fission and absorption reaction rates of MC and the errors of RH and SRH against MC. The detailed local 3D ring-wise reaction rates are not presented due to the vastness of data. Instead, the maximum and RMS errors of the local 3D as well as the axially-integrated 2D ring-wise reaction rates are summarized in Table VI. Lastly, Figure 3-6 presents the reference radially-integrated plane-wise fission and absorption reaction rates of MC in the active core region and the errors of RH and SRH against MC. Note that for the ring-wise reaction rates, only the fuel assemblies are of interest, while the plane-wise reaction rates include all the assemblies.

In terms of eigenvalues, RH clearly performs better than SRH: the eigenvalue error of RH against MC is only 80 pcm, while that of SRH is three times larger. However, they do not present meaningful differences when it comes to the reaction rate comparison with MC. In the fission reaction rates, RH does show slightly improved results than SRH: the maximum and RMS errors of RH against MC are lower than those of SRH by about 0.25% and 0.15%, respectively. In the absorption reaction rates, however, it is hard to claim that one scheme is better than the other. Their errors are also very similar in the radially-integrated plane-wise reaction rates. Nevertheless, SRH shows the characteristic intra-assembly error shapes while RH presents more-or-less flat error distributions in each assembly. Therefore, SRH can still provide reasonably accurate solutions in the average sense and can be a valid option if aggressive memory usage and runtime reduction are required, but RH would be more desirable in that it is more physically consistent with FH.

Table V. Comparison of eigenvalues between MC, RH, and SRH for the 3D full core. The values in the parentheses are the standard deviation for MC and the errors against MC for RH and SRH, all in pcm.

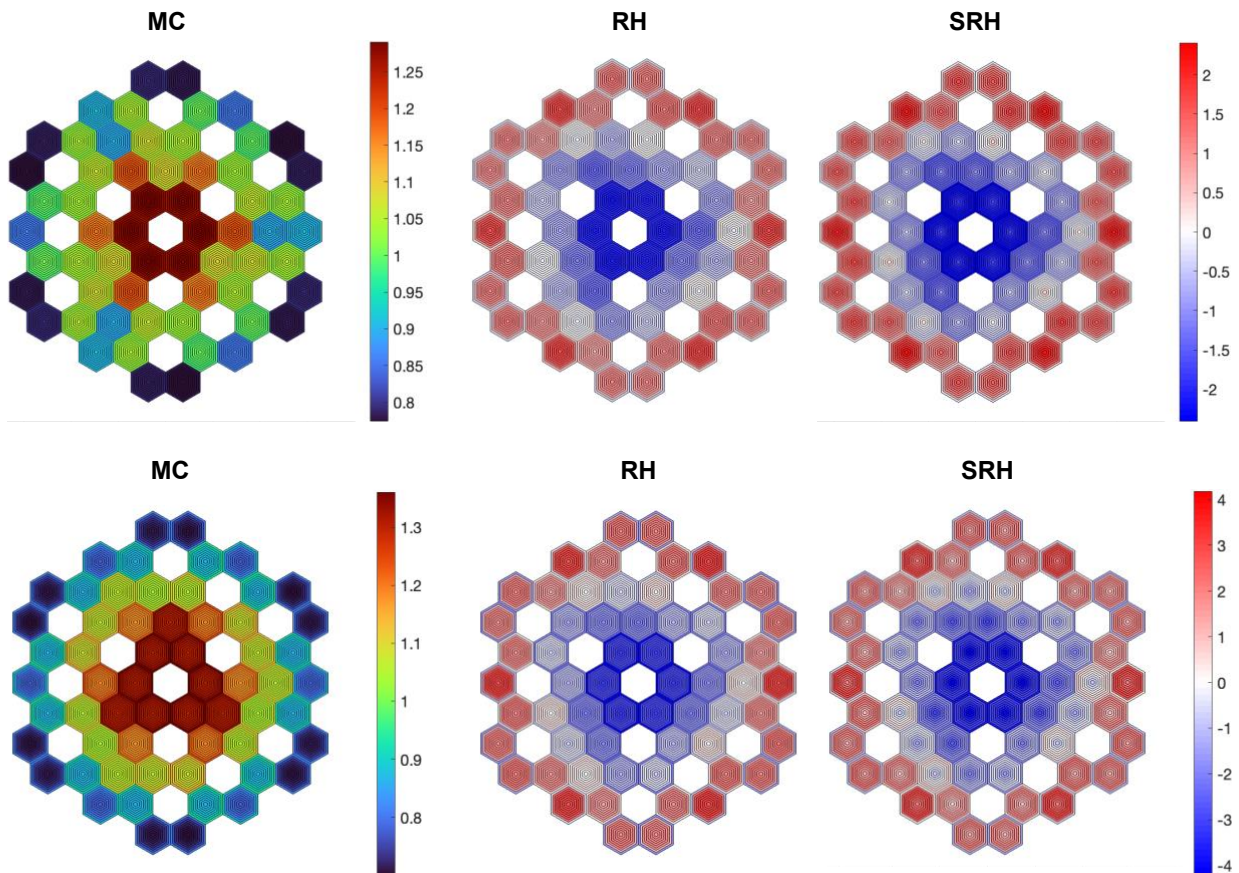| Case	MC	RH	SRH
Eigenvalue	1.03288 ($\pm$ 1)	1.03368 (80)	1.03535 (247)

Figure 3-5. Axially-integrated ring-wise fission (top) and absorption (bottom) reaction rates of MC and errors (%) of RH and SRH against MC for the 3D full core.

Table VI. Summary of 2D and 3D maximum and RMS errors (%) of ring-wise fission and absorption reaction rates for the 3D full core.

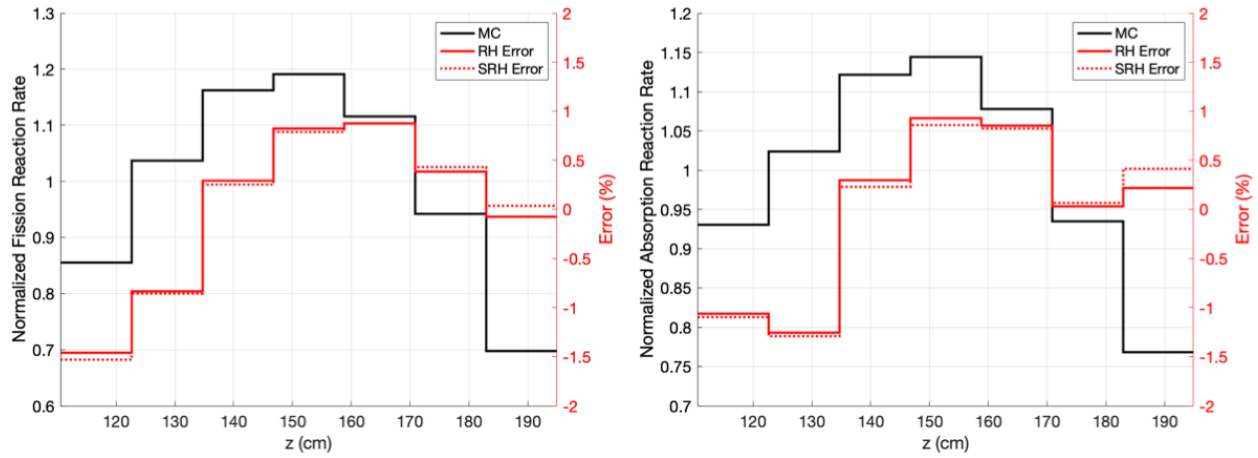| Reaction	Fission		Absorption	
Case	RH	SRH	RH	SRH
2D Max	2.15	2.40	4.04	4.18
2D RMS	1.01	1.17	1.75	1.76
3D Max	3.72	3.96	6.10	5.95
3D RMS	1.31	1.45	1.95	1.97

Figure 3-6. Radially-integrated plane-wise fission (left) and absorption (right) reaction rates of MC and errors (%) of RH and SRH against MC for the 3D full core.

4. CONCLUSIONS

The ring-heterogeneous approximation used in Griffin to efficiently analyze SFRs with unstructured meshes was introduced and verified. The ring-heterogeneous approximation was devised with multiphysics analysis in mind. Considering that the most important feedback mechanism in SFRs is the expansion of materials, the ring-heterogeneous approximation cleverly retains the heterogeneity of materials to allow their explicit deformation by casting an array of pins into the bands of materials composing the pins. Two variants of the ring-heterogeneous approximation were studied – the exact scheme and the simple scheme – depending on whether the topology of the original geometry is preserved. Even the exact scheme could reduce the number of elements significantly from a fully-heterogeneous mesh by a factor of 70 for the 2D full core problem, and the simple scheme could cut down the number of elements further by more than 20%.

Verification results with single assembly and full core problems of the ABTR benchmark demonstrated that the ring-heterogeneous approximation is a reasonable approximation for SFRs from a neutronics standpoint. Especially, the exact scheme yielded almost identical results with the fully-heterogeneous meshes in terms eigenvalues and reaction rates in both single assembly and full core problems. The simple scheme, on the other hand, presented relatively larger eigenvalue and reaction rate errors overall, which originate from the alteration of the geometric topology that changes the self-shielding effect from the original geometry. As the result, about 120 pcm of eigenvalue error and 1% of the maximum absorption reaction rate error were observed in the 2D full core problem, along with a small degree of in-out tilt of about ± 0.3% in the fission

reaction rate error distribution. Still, these errors are not generally considered significant in magnitude. The effect of topology change in the simple scheme was also observed in the 3D full core problem, although in the overall errors against Serpent, the two schemes did not present meaningful differences except for the eigenvalues. Hence, the simple scheme is considered "practically" accurate in the average sense. The exact scheme is still desirable in that it is more rigorous and physically consistent with the fully-heterogeneous mesh, but the simple scheme can become an option if aggressive optimization is required.

This work lays the foundation and provides confidence for the future multiphysics analysis by identifying the accuracy of the ring-heterogeneous approximation. Therefore, future work will include demonstrating and verifying the Griffin multiphysics calculations for SFRs using the ring-heterogeneous approximation. Each multiphysics code will use different mesh that is suitable for the code and its solution will be projected to the ring-heterogeneous neutronics mesh leveraging the MOOSE transfer system. Generating the fully-heterogeneous reference solutions for the 3D full core problem with more performance and memory usage optimization of Griffin will be another area for future work. In fact, the comparison with continuous-energy MC solutions involves numerous factors contributing to errors starting from the multi-group cross sections. Therefore, having a fully-heterogeneous reference on the same code basis for more rigorous verification is desired. In addition, studies on the impact of control rods and group structures will be required as well.

REFERENCES

1. TerraPower, "Natrium™ Reactor and Integrated Energy Storage," https://www.terrapower.com/our-work/natriumpower.
2. C. Lee et al., "Griffin Software Development Plan," INL/EXT-21-63185 & ANL/NSE-21/23, Idaho National Laboratory & Argonne National Laboratory (2021).
3. A. Lindsay et al., "2.0 – MOOSE: Enabling Massively Parallel Multiphysics Simulation," SoftwareX **20**, no. 101202 (2022).
4. V. Labouré et al., "Improved Multiphysics Model of the High Temperature Engineering Test Reactor for the Simulation of Loss-Of-Forced-Cooling Experiments," Annals of Nuclear Energy **189**, no. 109838 (2023).
5. S. Terlizzi and V. Labouré, "Asymptotic Hydrogen Redistribution Analysis in Yttrium-Hydride-Moderated Heat-Pipe-Cooled Microreactors Using DireWolf," Annals of Nuclear Energy **186**, no. 109735 (2023).
6. S. Schunert et al., "An Equilibrium Core Depletion Algorithm for Pebble-Bed Reactors in the Griffin Code," Annals of Nuclear Energy **192**, no. 109980 (2023).
7. J. Hader, E. Shemon, C. Lee, "Initial Verification of Heterogeneous Multigroup Cross Sections in MC^2-3/PROTEUS," Transactions of the American Nuclear Society **111**, pp. 1213-1216 (2014).
8. T. K. Kim, "Benchmark Specification of Advanced Burner Test Reactor," ANL/NSE-20/65, Argonne National Laboratory (2020).
9. C. Lee, W. S. Yang, "MC^2-3: Multigroup Cross Section Generation Code for Fast Reactor Analysis," Nuclear Science and Engineering **187**(3), pp. 268-290 (2017).
10. J. Leppänen et al., "The Serpent Monte Carlo Code: Status, Development and Applications in 2013," Annals of Nuclear Energy **82**, pp. 142-150 (2015).